Heterogeneous magnetism and kinetic arrest in antiperovskite $Mn_{3-x}Ni_xGaC$ compounds with Ni_2MnGa Heusler insertions

Ö. Çakır
Physics Department, Yildiz Technical University, Istanbul, Turkey

E. Dias and K. R. Priolkar
Department of Physics, Goa University, Taleigao Plateau, Goa 403206, India

A. Hoser
Helmholtz-Zentrum Berlin für Materialien und Energie Hahn-Meitner-Platz 1, 14109 Berlin Germany

M. Farle and M. Acet*
Faculty of Physics, Duisburg-Essen University, D-47057 Duisburg, Germany

(Received 6 February 2020; revised 4 June 2020; accepted 2 July 2020; published 20 July 2020)

Mn-based antiperovskite compounds in the form Mn_3AX, where A is a main group element and X is C or N, undergo magnetostructural transitions with which these materials acquire magnetocaloric, giant magnetoresistance, and spin-transport properties, which can be modified or tailored by manipulating the compositions of numerous compounds. This enables closer investigations and better understandings of the underlying principles governing these properties. $Mn_{3-x}Ni_xGaC$, which is a derivative of the prototype Mn_3GaC antiperovskite, would normally be expected to form a cubic structure with a homogeneous composition. Contrary to this, we find that the addition of Ni leads to a heterogenous compound consisting of an antiperovskite part and a Ni_2MnGa Heusler insertions. The system shows kinetic arrest features, which we study as a function of Ni composition using the techniques of x-ray diffraction, magnetization, and neutron diffraction under a magnetic field.

DOI: 10.1103/PhysRevB.102.024431

I. INTRODUCTION

Nitrides and carbides of transition metals and alloys are interstitial compounds in which C and N take up positions located at octahedral or tetrahedral sites in various crystal structures. Stable 3*d* transition-metal carbides and nitrides form in elements lying left of Co in the periodic system, and as of Ni, stable 3*d* interstitial compounds are not found or are either difficult to stabilize or are metastable in metals up to Zn. The reason for this is because interstitial C or N requires from the host-metal a *d*-band that has sufficient space for the *p*-electrons of the interstitial atoms to hybridize and build a compound [1,2].

Among the 3*d* metals, Mn and Fe in their fcc structure are particularly important in relation to accommodating interstitials. It is long-known that these metals readily form the stable compounds Mn_4N and Fe_4N. More recently, it was reported that Mn_4C can also be stabilized [3–5]. Fe_4C is not stable, however, much theoretical work has been carried out on this system, and it has been shown that some derivatives of this system containing doped elements can be stabilized as an antiperovskite compounds [6–10].

Fcc-Mn and fcc-Fe with C or N form the basis of the important class of magnetic antiperovskite compounds M_3AX, where M is Mn or Fe, A is a metal or a semi-metal in groups 12 to 15 of the periodic system, and X is C or N. Early detailed reviews and current works are available on the basic properties of the magnetic states and structural and magnetic transitions in a broad range of M_3AC and M_3AN compounds [10–17]. Here also, the binding of the interstitial is accomplished over the hybridization of the *p*-electrons of the interstitials with the host M–A *d*-band. More recently, however, M as Ni is also attracting attention because of the presence of superconducting properties appearing in some Ni-based antiperovskites [18–23]. The binding of the interstitial atom in the Ni-based antiperovskites is usually accomplished over the *p*-bands of the A and X species as suggested by the density of states determined for various compounds [24–27]. Nevertheless, the presence of a stable Ni_3GaC or a Ni_3GaN compound has until now not been reported.

More recent studies on Mn-based antiperovskites have revealed other detailed properties such as the occurrence of deviations from ideal cubic positions of the atoms [28,29] and nonergodic effects at the magnetostructural phase transitions with inverted hysteresis loops [30]. It appears, therefore, that there is much more to be investigated to be able to understand many more underlying principles that govern the properties of these systems.

A material that particularly stands out among the antiperovskites with its antiferromagnetic (AF) to ferromagnetic (FM) magnetostructural transition at 160 K is Mn_3GaC. The

*mehmet.acet@uni-due.de

presence of this transition has been the source of many studies particularly related to magnetocaloric effects as well as to the properties of the magnetostructural transition itself [31–34]. Although many combinations by gradually varying the *A*-species of this material have been studied, substituting Mn by other 3*d* elements in Mn_3GaC has been less studied [10,35]. Ni_3GaC is not stable. Therefore, to understand how the properties of Mn_3GaC would develop as the composition of the unstable compound Ni_3GaC is approached, we substituted progressively small amounts of Ni for Mn and examined the destabilization of the pure antiperovskite phase and the evolution of the magnetic properties along with emerging kinetic arrest effects related to the presence of magnetic inhomogeneities.

II. EXPERIMENT

Polycrystalline samples of $Mn_{3-x}Ni_xGaC$ with $x = 0.1$, 0.2, 0.5, and 1.0 were prepared by mixing Mn and Ni powders, Ga pieces, and graphite powder in stoichiometric proportions and pressed into a pellets. The pellet was sealed in a quartz tube under argon atmosphere, and the sample was held at 850° C for five days to undergo a solid-state reaction. The pellet was then grinded, repressed into a pellet, and fired at 850° C for a further five days, and this was repeated two times. The Mn-Ni/Ga proportions were determined by using energy dispersive x-ray spectroscopy. The magnetization measurements were carried out using a superconducting quantum interference device magnetometer. X-ray diffraction (XRD) studies were carried out at room temperature with Cu-Kα radiation. Neutron diffraction experiments were performed on the E6 spectrometer at Helmholtz-Zentrum Berlin using a wavelength of 2.45 Å in conjunction with a superconducting magnet. The sample was placed in an aluminum container. Rietveld analysis was carried out on both x-ray and neutron diffraction using FULLPROF software [36].

III. RESULTS

We present first the XRD data for $Mn_{3-x}Ni_xGaC$ and examine the strain properties. We then present the results of the magnetization measurements for both systems and finally, the results on neutron diffraction studies carried out in magnetic fields.

A. X-ray diffraction

The refined XRD data are shown in Figs. 1(a) and 1(b) for $x = 0.1$ and $x = 0.2$, respectively. In addition to the peaks associated with the antiperovskite compound, peaks related to the cubic Heusler structure of Ni_2MnGa are also observed (marked with an asterisk). MnO is also present.

The situation is similar in Fig. 2 for $x = 0.5$ [Fig. 2(a)] and $x = 1.0$ [Fig. 2(b)], except that the peaks related to the Heusler structure are now broader. In addition to the broadening, a cubic phase corresponding to a lattice parameter of 3.683 Å appears. This can be related to the presence of a Ni-rich fcc Ni-Mn phase. MnO is absent in this case.

In all cases, the lattice parameters of the antiperovskite is 3.888 ± 0.005 Å corresponding to the lattice parameter of Mn_3GaC. The lattice parameter for the identified Heusler

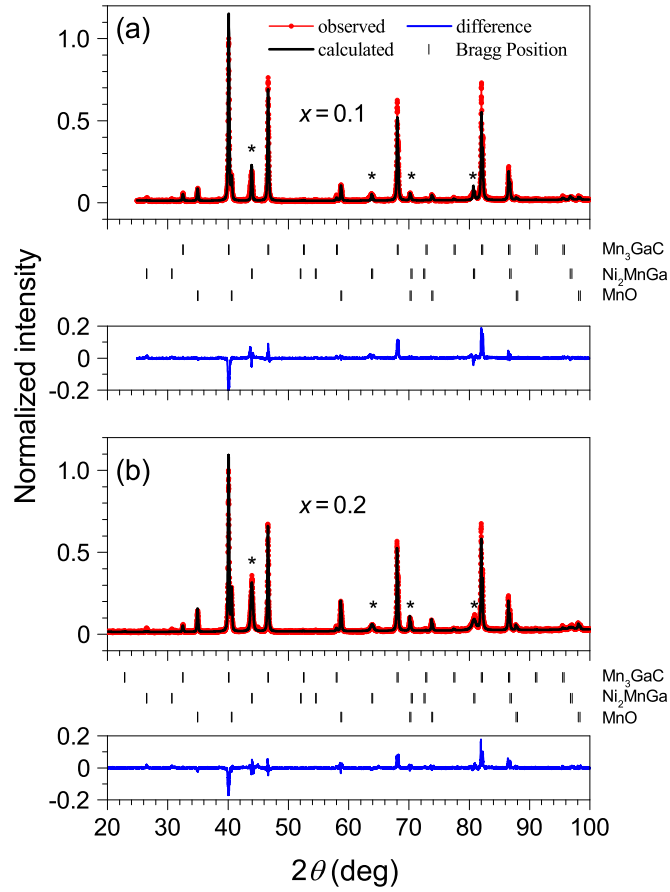

FIG. 1. Refined XRD data for $Mn_{3-x}Ni_xGaC$ for (a) $x = 0.1$ and (b) 0.2. The asterisks correspond to the position of the Heusler peaks.

structure is 5.833 Å which is in good agreement with that of Ni_2MnGa. The phase fractions obtained from the analyses are collected in Table I. As seen from the table, there is a tendency of the Heusler quantity to increase as the Ni concentration increases, particularly for $x = 0.1$, 0.2, and 1.0. The deviation for $x = 0.5$ is because of the uncertainties in the analysis due, in particular, to the weak Heusler peaks.

The broadening of the peaks indicate that strain develops as the Ni concentration, and therefore, the amount of Heusler phase increases. The developing strain is associated with the lattice mismatch of the Heusler and the antiperovskite. The full-width at half-maxima (FWHM) corrected to the instrumental broadening are plotted as a function of Ni concentration in Fig. 3. The FWHM of the peaks corresponding to the antiperovskite structure, indicated as AP in the figure, for $x = 0.1$ and 0.2 are identical to the instrumental broadening determined with a Si standard. The Heusler peaks (H) for these two compositions are broader. For $x = 0.5$ and 1.0, the AP peaks themselves become broader. Their corresponding H-peaks become so broad that they are plotted in the inset on another scale. For the lower two Ni concentrations, accommodating a Heusler insertion causes first strain in the insertion itself and not in the antiperovskite. For the higher Ni-concentrations, not only the Heusler insertion but the entirety of the sample is under strain. Broadening of the Heusler peaks for the lower two Ni-concentrations could be occurring due to additional size-effects next to strain-effects when the Heusler

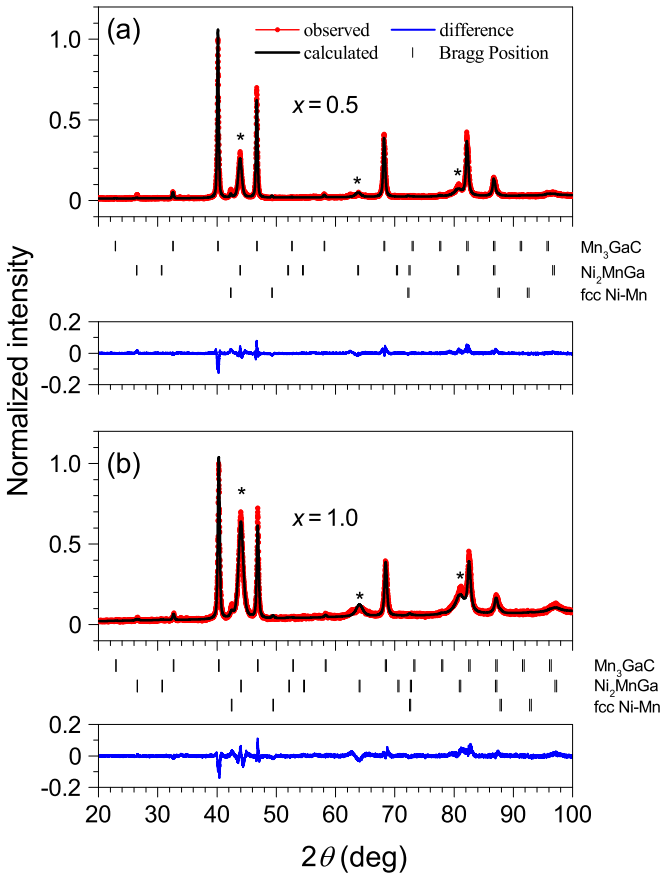

FIG. 2. Refined XRD data for $Mn_{3-x}Ni_xGaC$ for (a) $x = 0.5$ and (b) 1.0. The asterisks correspond to the position of the Heusler peaks.

insertion is small. However, since the FWHM of the H-peaks increases with increasing Ni concentration and thereby the insertions are not getting smaller, the increase of the width would be due entirely to strain.

B. Magnetization

We present here the data on the temperature and field dependencies $M(T)$ and $M(B)$ for the individual samples of $Mn_{1-x}Ni_xGaC$. $M(B)$ are obtained in the first quadrant only.

1. x = 0.1

$M(T)$ for $x = 0.1$ measured in various fields are shown in Fig. 4. Figure 4(a) shows $M(T)$ measured in a 5-mT field in a zero-field-cooled (ZFC), field-cooled (FC), and field-warming (FW) sequence. The whole of $M(T)$ is reminiscent of the data

TABLE I. Percent phase fractions of components present in the compounds.

x	Antiperovskite %	Heusler %	MnO %	Fcc Ni-Mn %
0.1	77.9	9.2	12.9	–
0.2	60.0	19.7	20.3	–
0.5	73.9	24.7	–	1.4
1.0	50.4	47.5	–	2.1

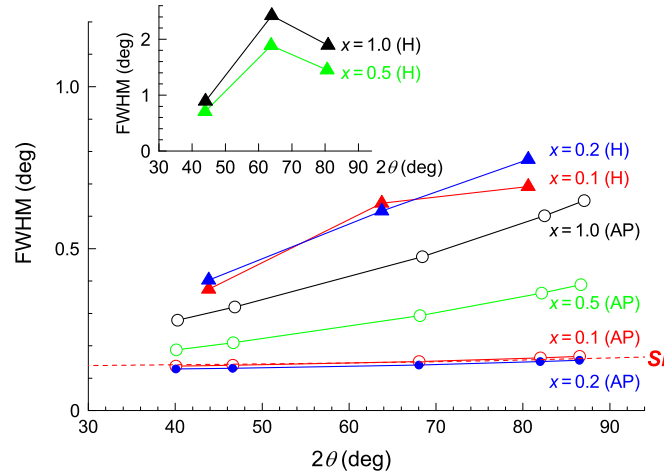

FIG. 3. FWHM vs. 2θ for $Mn_{3-x}Ni_xGaC$. The instrumental broadening is determined with a Si standard.

for Mn_3GaC featuring a drop with decreasing temperature at the first-order FM-to-AF magnetostructural transition around T_i. For Mn_3GaC, this occurs at 160 K, so that adding Ni enhances FM exchange and causes T_i to decrease down to about 120 K. The hysteresis around T_i in $M(T)$ is about 10 K, which is broader than the 3 K-hysteresis in Mn_3GaC.

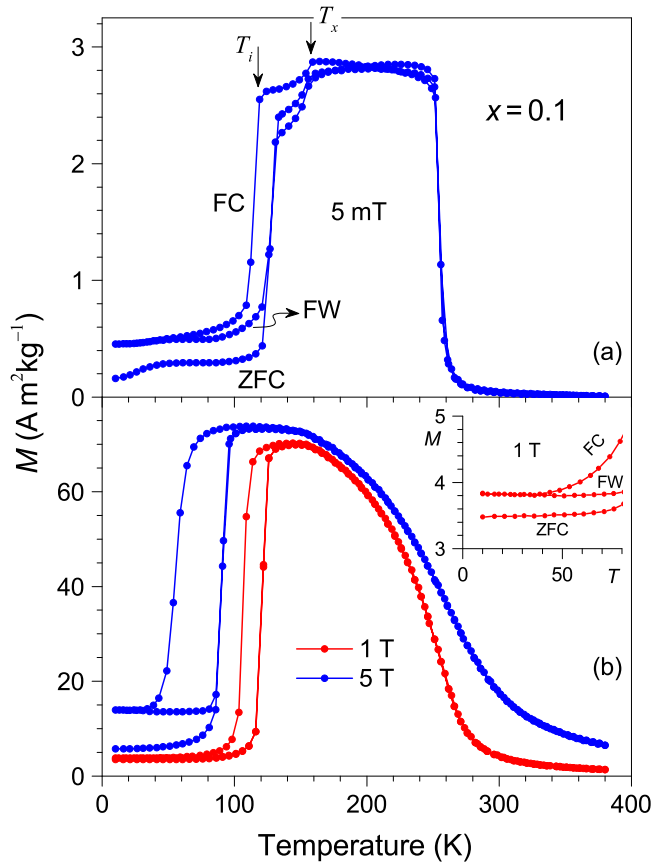

FIG. 4. ZFC, FC, and FW $M(T)$ for $Mn_{2.9}Ni_{0.1}GaC$ measured in (a) 5 mT and (b) 1 and 5T. Inset in (b) is an expanded plot of the 1 T measurements at low temperature showing the splitting.

This is due to the increased strain when the Ni concentration increases; in agreement with the line-broadening observed in the XRD studies. The other feature is the drop in $M(T)$ occurring at the transition from the FM to the paramagnetic (PM) state at the Curie temperature $T_C = 260$ K. This is somewhat higher than $T_C = 250$ K for Mn_3GaC; so that here also we see that introducing Ni strengthens the FM exchange. All curves merge around T_C.

Another feature seen in $M(T)$ of the $x = 0.1$ sample that is not present in Mn_3GaC is the wavy behavior between 120 and 160 K. The ZFC-$M(T)$ shows a weak temperature-dependence at low temperatures and rises sharply around T_i, but then the rise slows down as it approaches the demagnetization limit at the temperature designated as T_x. T_x lies at 160 K, which actually marks the AF/FM transition in Mn_3GaC. It remains at the same value for all measurement sequences and is an indication of the presence of Mn_3GaC regions apart from the Ni_2MnGa Heusler inclusions. The expected cause of this property is discussed in more detail in Sec. IV.

At high temperatures, FC-$M(T)$ is the same as the ZFC- and FW-$M(T)$s with all curves showing similar behavior in the PM and FM ranges. Some small deviations occur in the range of the demagnetization limit after the temperature is decreased to below T_C down to T_x. However, after the AF state sets in at T_i and $M(T)$ drops, $M(T)$ runs almost at a constant value down to the lowest temperature with a background magnetization that is not present in the PM state. This indicates that some residual FM coupling is present at these temperatures after the sample is cooled through T_i in a field as little as 5 mT. It is also seen that the background in the ZFC case is less.

To further examine these features, we measured $M(T)$ in higher magnetic-fields of 1 and 5 T. The results are shown in Fig. 4(b). It turns out that the wavy feature becomes suppressed while the difference between the ZFC $M(T)$ and the other two measurement sequences, FC and FW, below T_i become enhanced with respect to the 5 mT-$M(T)$. The enhancement increases with increasing measuring field. The low-temperature details for the 1 T measurements are given in the inset. For the measurement under 1 T, $T_i = 120$ K, which is the same value when measured under 5 mT [Fig. 4(a)]. The shift becomes more distinct with T_i reaching down to 60 K when measured under 5 T. The hysteresis around T_i also broadens and the difference between ZFC and FC or FW measurements enhance further. This enhancement as well as the strong shift in T_i to lower temperatures are indications of kinetic arrest and is discussed further in Sec. IV.

We next turn to the magnetic-field-dependence of the magnetization $M(B)$ shown in Fig. 5 for the ZFC case, where the sample is cooled through T_C in zero-field prior to the measurement in an increasing-decreasing-field sequence. In Fig. 6, we show the FC-case for $M(B)$, where the sample is cooled through T_C in a field of 5 T and then measured in a decreasing-increasing-field sequence.

For the ZFC case in Fig. 5(a), with $M(B)$ obtained at 10 K, the curve appears to be retraceable at high fields, and a hysteresis between increasing and decreasing fields is observed at lower fields. In Fig. 5(b), a difference at high-fields between increasing and decreasing field $M(B)$s begins to appear faintly at 30 K. This difference becomes more obvious

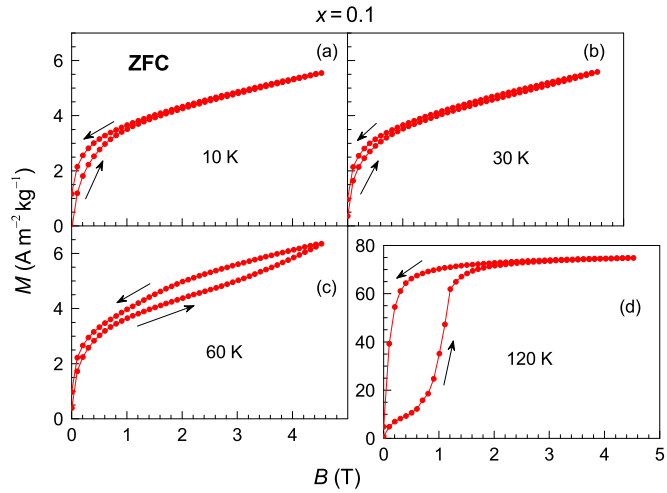

FIG. 5. ZFC $M(B)$ from 300 K for $Mn_{2.9}Ni_{0.1}GaC$ at (a) 10, (b) 30, (c) 60, and (d) 120 K. Arrows indicate the field-change directions.

in Fig. 5(c) at 60 K, where an up-turn in the increasing-field curve begins to appear at around 2 T, indicating the beginning of a field-induced reverse-transformation to the FM state. The reverse transformation is not complete since there is no high-field-range where $M(B)$ is retraceable so that the curve is a partial minor loop. The values of $M(T)$ at the maximum 5-T field in Figs. 5(a) to 5(c) correspond to the values of $M(T)$ at 10 K in Fig. 4(b) obtained under 5 T. In Fig. 5(d), the field-induced reverse-transformation to the FM state at 120 K becomes distinct, and the value of $M(T)$ in 5 T reaches to that corresponding to a value in the FM state seen in Fig. 4(b).

Figure 6(a) shows the case when the sample is cooled in 5 T through T_C down to 10 K. The system becomes partially locked in the FM state from 5 T down to about 4 T with $M(T) = 14$ Am^{2}kg^{-1}, which corresponds to the FC-$M(T)$ at 10 K in Fig. 4(b). As the field is lowered to below 4 T,

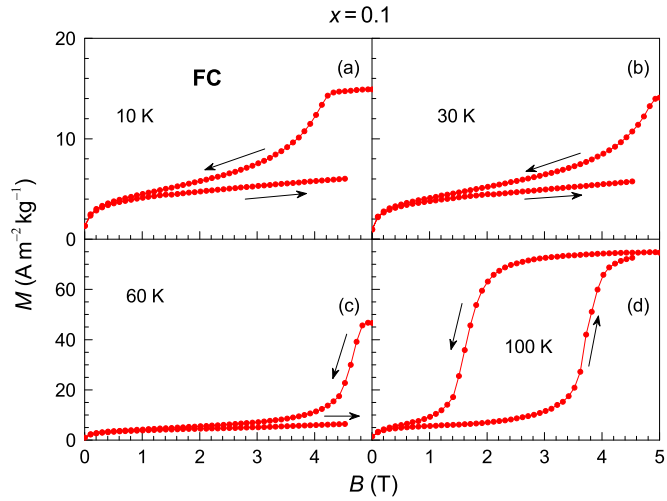

FIG. 6. FC $M(B)$ from 300 K for $Mn_{2.9}Ni_{0.1}GaC$ at (a) 10, (b) 30, (c) 60, and (d) 100 K. Arrows indicate the field-change directions. The-increasing field branches are nearly identical to the increasing-field branches of the ZFC data in Fig. 5.

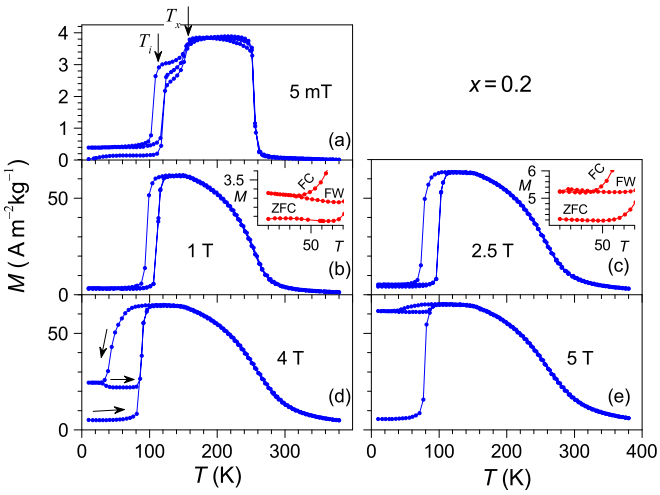

FIG. 7. ZFC, FC, and FW $M(T)$ for $Mn_{2.8}Ni_{0.2}GaC$ measured in (a) 5 mT, (b) 1 T, (c) 2.5 T, (d) 4 T, and (e) and 5 T. Insets in (b) and (c) are an expanded plot of the measurements at low temperature showing the splitting.

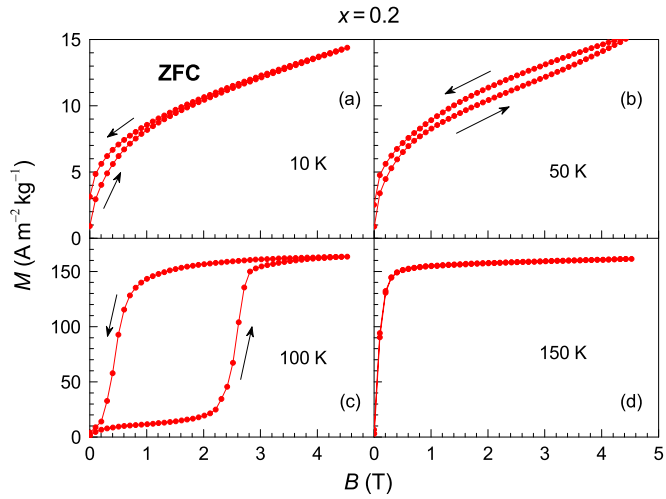

FIG. 8. ZFC $M(B)$ from 300 K for $Mn_{2.8}Ni_{0.2}GaC$ at (a) 10, (b) 50, (c) 100, and (d) 150 K. Arrows indicate the field-change directions.

$M(B)$ begins to decrease rapidly as the state of the system approaches that of the ZFC-state in Fig. 4(b). This is better seen when the field is increased back to 5 T, where the value of $M(T)$ remains at about $M(T) = 6\ \mathrm{Am^2kg^{-1}}$ corresponding to the value in the ZFC state. A full reverse transformation would require higher fields than that available for these experiments. The case is similar to Figs. 6(b) and 6(c) at 30 and 60 K, respectively.

2. x = 0.2

Increasing slightly the Ni composition from $x = 0.1$ to $x = 0.2$ (from 2 at% Ni to 4 at% Ni) has no effect on T_C, but T_i drops down to 113 K due to a small enhancement in the FM exchange. However, this small compositional change leads to pronounced changes in the kinetic arrest properties. The data shown in Fig. 7 resemble those shown in Fig. 4. However, here the difference in the ZFC and FC or FW curves increases more rapidly as the measuring field increases as shown in Figs. 7(a) to 7(e). At 5 T, the FM state is arrested almost completely. We also see that the thermal hysteresis around the transition broadens as the measuring field increases. This is expected to be due to enhanced strain caused by the interaction of the external field and the Heusler inclusions (see Sec. IV).

A series of ZFC $M(B)$ measurements are shown in Fig. 8. The development of the hysteresis and the field-induced reverse transformation from Fig. 8(a) to 8(d) is similar to that of the $x = 0.1$ sample shown in Fig. 4. However, what is seen here in better detail in Fig. 9(a) to 9(d) is that reincreasing the field from 0 to 5 T keeps $M(B)$ on the ZFC curve at 10 and 50 K so that only a partial minor loop can be attained with the available 5-T field. On the other hand the forward and reverse transformations are complete at 100 K. At 150 K [Fig. 9(e)], the system is fully in the FM state.

3. x = 0.5 and 1.0

As the Ni content further increases to $x = 0.5$, T_C increases to 320 K and becomes smeared out in a broader temperature range than for $x = 0.1$ and 0.2 as seen in Figs. 10(a) and 10(b). 320 K corresponds to T_C of Ni_2MnGa, indicating that the Heusler entities become large enough to be able to compete with the main Mn_3GaC surrounding matrix. The smearing of T_C becomes more evident in Figs. 10(c) to 10(f) as the measuring field increases, and the FM interactions of Mn_3GaC with $T_C = 260$ K also enhance due to the external field and the internal field of the Heusler component. The onset of the splitting between the ZFC and FC or FW curves begins now just below T_C. This is because different spin configurations can be stabilized whether the system is cooled under field or without field to a state with mixed FM exchanges arising from the antiperovskite and Heusler components. The transition around T_i becomes less distinct but can still be found to be at around 120 K. The FM exchange is now stronger so that the FM state becomes almost completely arrested at 3 T. $M(T)$ runs nearly temperature-independent below 100 K for

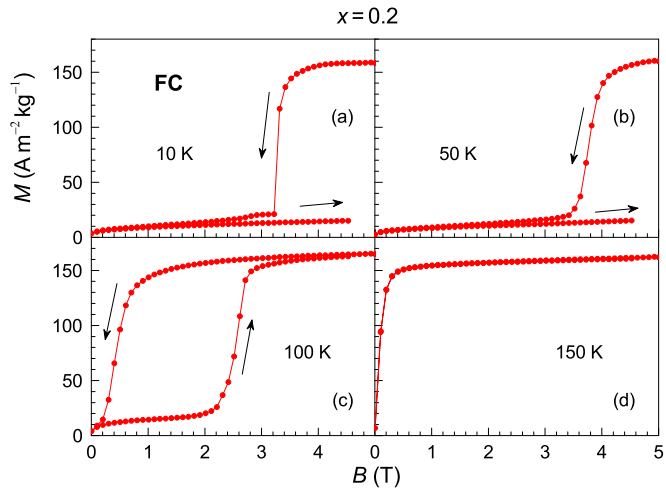

FIG. 9. FC $M(B)$ from 300 K for $Mn_{2.8}Ni_{0.2}GaC$ at (a) 10, (b) 50, (c) 100, and (d) 150 K. Arrows indicate the field-change directions. The increasing field branches are nearly identical to the increasing-field branches of the ZFC data in Fig. 8.

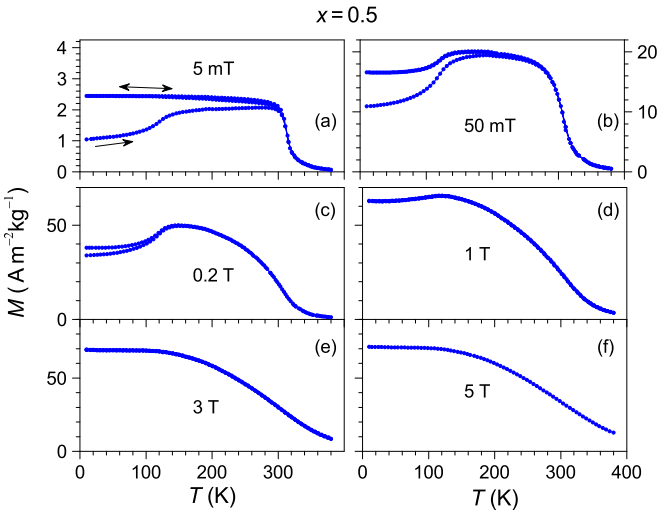

FIG. 10. ZFC, FC, and FW $M(T)$ for $Mn_{2.8}Ni_{0.2}GaC$ measured in (a) 5 mT, (b) 50 mT, (c) 0.2 T, (d) 1 T, (e) 3 T, and (f) 5 T.

3 and 5 T indicating that the presence of AF exchange still hinders a steady increase in the magnetization with decreasing temperature.

These effects are more pronounced in the sample with $x = 1.0$, for which $M(T)$ is shown in Figs. 11(a) to 11(c). The splitting occurring below T_C is shifted to lower temperatures as the measuring field increases and eventually the high-temperature state becomes fully arrested down to the lowest temperatures.

C. Neutron diffraction

To examine the kinetic arrest more closely we carried out neutron diffraction experiments under magnetic field by cooling the sample through the transition temperature under various conditions described below. The experiments were carried out on the $x = 0.2$ sample, which shows the kinetic arrest features more distinctly (Fig. 7). The results are shown in Fig. 12. The sequence of measurements are given from 1 to 5 in the legend. The sample was first cooled from room temperature to 150 K in a zero field, and a pattern was recorded. The sample at this temperature is in the FM state. Then, a field of 6 T was applied and the pattern was recorded again. There is no difference in these two data. The sample was then taken down to 33 K without removing the 6-T magnetic field. In this case, a peak appears which is related to the AF ordering of MnO occurring below 116 K. There is no indication of any other antiferromagnetism. However, when the field is removed, an AF peak belonging to the antiperovskite structure appears at around 30.5°. These results are in agreement with the $M(B)$ measurements shown in Fig. 9 showing that the FM state is retained at low temperatures as long as the field remains applied. On removing the field the system reverts to the AF state. In steps 3 and 4, there is also a broadening of the Heusler peak, which narrows again when the temperature is brought back up to 150 K in step 5.

IV. DISCUSSION

The combination of magnetization, XRD, and field-dependent neutron diffraction studies on $Mn_{3-x}Ni_xGaC$

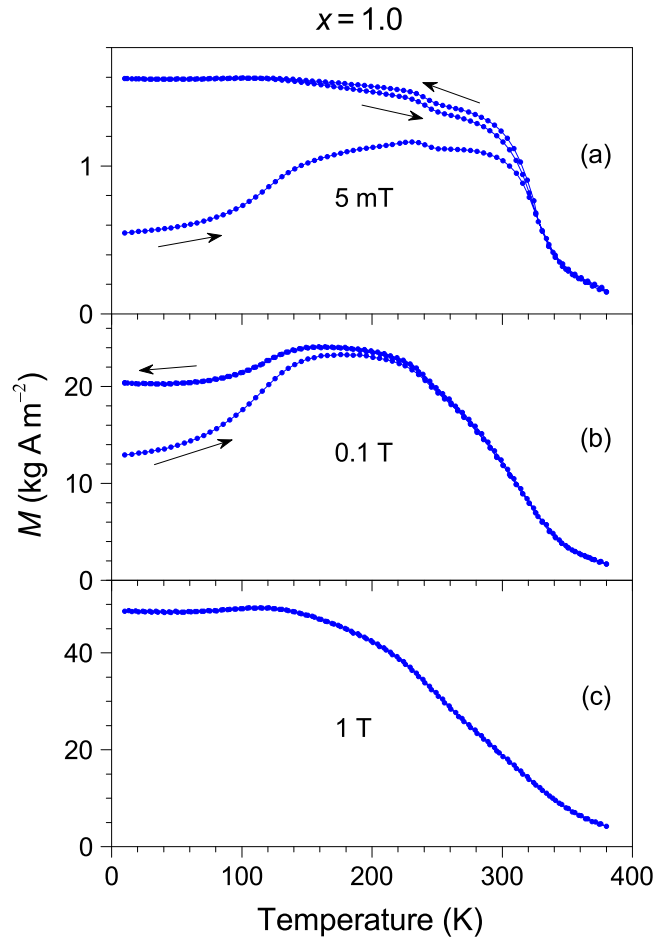

FIG. 11. ZFC, FC, and FW $M(T)$ for $Mn_{2.0}NiGaC$ measured in (a) 5 mT, (b) 0.1 T, and (c) 1 T.

shows that instead of having a uniform antiperovskite, a heterogenic system composed of an antiperovskite and a Heusler component stabilizes. If this were due to carbon deficiency, so that Heusler regions were built around carbon-deficient sites, then the amount of the Heusler should have remained

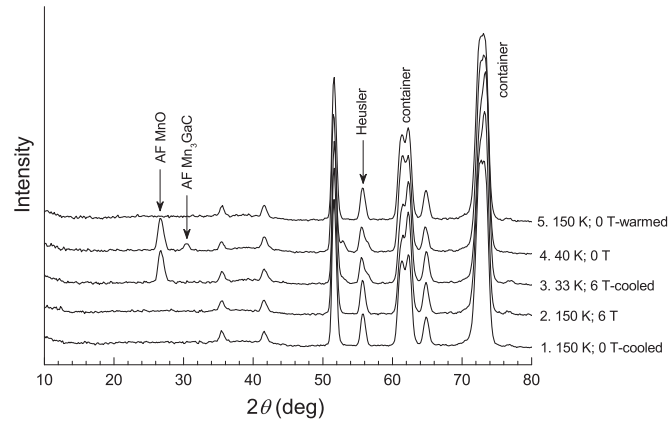

FIG. 12. The results of neutron diffraction experiments carried out in the sequence given in the legend. The Al peaks from the sample container and the magnet frame are split due to their different positions in the setup.

constant with increasing Ni concentration. This is not the case here as observed in the XRD and the magnetization data. Instead, another mechanism for the development of Heusler regions should be considered. If Ni and Mn are not ideally distributed and Ni has other Ni atoms as nearest neighbors, a locally unstable Ni_3GaC configuration becomes unfavorable with respect to the formation of Ni_2MnGa by excluding the C. The C exclusion mechanism, in this case, can be due to the incapability of accommodating C in a local Ni environment—the same reason why Ni-carbides are not stable as mentioned in Ssec. I. Interstitials are little accommodated in Co [37] and are not accommodated in transition metals to the right of Co in the periodic system, i.e., for a valence electron concentration $(e/a) \geqslant 9$ [(e/a): sum of s- and d-electrons]. Carbides are readily formed when there is sufficient space in the d-band of the host metal to accommodate the p-electrons donated by the interstitial C [2]. This is valid for $(e/a) \leqslant 8$, namely for the elements beginning with Fe and those to its left and can be seen in many of the calculated partial density of states, where the p-states of C and the d-states of the host metal overlap and provide a means for bonding [38–41]. In Ni-rich regions, (e/a) would locally be closer to 10— e/a of Ni—so that these regions cannot accommodate C as an interstitial. This picture can also account for the increasing amount of the Heusler component with increasing Ni concentration, leading to the effects observed in the magnetization and in the kinetic arrest process.

The effect of mixed exchange arising from the antiperovskite and Heusler components can already be observed in the sample with $x = 0.1$. The appearance of a T_x is an indication of competing internal fields. The Mn_3GaC antiperovskite component has its own transition at $T_i = 160$ K, and here, this coincides with T_x. This transition carries its traces in $M(T)$ for both $x = 0.1$ and 0.2 (Sec. III B). However, the transition is not complete at this temperature with $M(T)$ remaining at high values. It would have normally dropped to vanishing values as in Mn_3GaC, but it is kept at higher values by the internal field of the FM Ni_2MnGa Heusler inhomogeneity until a driving force is reached at a lower temperature where the FM state can no longer be sustained. This defines T_i. The effect of the internal field of the Heusler on the AF/FM transition is observed only in small fields so that T_i and T_x can be distinguished. For an applied field of 1 T, T_i and T_x appear to coincide for both $x = 0.1$ and 0.2, and the effect of the internal field on $M(T)$ is masked. At higher fields, T_i shifts rapidly to lower temperatures as both the internal field of the FM Heusler and the external fields stabilize the FM state. At a higher Ni concentration of $x = 0.2$, there are more Heusler inclusions so that the effect of the internal field is enhanced so that the total internal and external field becomes sufficient to nearly suppress completely AF ordering down to the lowest temperatures [Fig. 7(e)]. The transition hysteresis also broadens due to induced strains resulting from coexisting AF and FM phases. At even higher Ni concentrations of $x = 0.5$ and 1.0, more FM Heusler inclusions are formed so that AF ordering is nearly altogether suppressed as seen in $M(T)$ in Figs. 10 and 11.

Replacing Mn with small amounts Ni leads to the formation of a heterogeneous system composed of antiperovskite Mn_3GaC and Heusler Ni_2MnGa. We find no composition-range in which a uniform antiperovskite compound forms. The antiferromagnetism of Mn_3GaC and the ferromagnetism of Ni_2MnGa gives rise to kinetic arrest effects, of which the properties vary rapidly with increasing Ni concentration. A kinetic arrest effect is also present in pure Mn_3GaC, which shows a shift of the transition temperature with applied magnetic-field at a rate of -4.4 KT^{-1} [32]. In the Ni-substituted samples this increases to -10 KT^{-1} for $x = 0.1$ and -13 KT^{-1} for $x = 0.2$. This indicates that the internal field of the Heusler inclusion, which is absent in pure Mn_3GaC, has a strong effect on the kinetic arrest properties of the alloys incorporating Ni. From these values we can estimate an internal field of 2.3 T for $x = 0.1$ and 3 T for $x = 0.2$. Therefore, for higher Ni Ni-concentrations the AF state is nearly fully suppressed.

There are very strong similarities in the kinetic arrest properties of $Ce(Fe_{0.96}Ru_{0.04})_2$ [42], C-deficient Mn_3GaC [43], $Mn_{1.82}Co_0.18Sb_{0.95}In_{0.05}$ [44], and the present $x = 0.2$ sample. The $M(T)$ data are qualitatively nearly the same so that the origin of the kinetic arrest in all of these systems can also be due to the presence of magnetic inhomogeneities. In fact, for C-deficient Mn_3GaC, it has been explicitly reported that the presence FM inhomogeneities is the cause of the observed magnetic kinetic arrest.

$Mn_{3-x}Ni_xGaC$ is probably not the only such heterogeneous antiperovskite/Heusler system and other $Mn_{3-x}A_xX$ systems can also be devised with other A and X species. The A-element can be chosen as one being with $e/a > 10$ so that interstitial atoms will not collect in its vicinity and form magnetic inclusions in an antiperovskite matrix having magnetic properties depending on the chosen X-element. In such a manner the magnetic interactions in the Heusler and the antiperovskite can be tailored to having various combinations of antiferromagnetism and ferromagnetism.

V. CONCLUSION

We prepared the $Mn_{3-x}Ni_xGaC$ antiperovskite/Heusler heterogeneous system with coexisting FM exchange provided by the Heusler inclusion Ni_2MnGa and the AF exchange provided by the antiperovskite Mn_3GaC and studied the magnetic and kinetic arrest properties. The heterogeneity is both structural and magnetic. We interpreted the heterogeneity to be caused by the exclusion of carbon from regions in the sample, where Ni-Ni neighborhoods prevent accommodating the carbon at interstitial sites. The presence of kinetic arrest in this system is due to its heterogeneous nature. Further similar antiperovskite/Heusler heterogenic systems can open up the possibility to introduce new materials and new magnetic interaction mechanism.

ACKNOWLEDGMENTS

This work was supported by Deutsche Forschungsgemeinschaft (Project No. 405553726-CRC/TRR 270). K.R.P. acknowledges financial support from Science and Engineering Research Board, Govt. of India under the Project No. EMR/2017/001437.

[1] W. Pepperhoff and M. Acet, *Constitution and Magnetism of Iron and its Alloys*, (Springer, Berlin, 2001), Chap. 5.

[2] T. Shigematsu, J. Phys. Soc. Jpn. **37**, 940 (1974).

[3] P.-Z. Si, X.-Y. Wang, H.-L. Ge, H.-D. Qian, J. Park, Y. Yang, Y.-S. Li, and C.-J. Choi, Nanomaterials **8**, 1056 (2018).

[4] P.-Z. Si, H.-D. Qian, H.-L. Ge, J. Park, and C.-J. Choi, Appl. Phs. Lett. **112**, 192407 (2018).

[5] P.-Z. Si, J. T. Lim, J. Park, and C.-J. Choi, Powder Diffr. **34**, 196 (2019).

[6] E. L. Peltzer y Bianca, J. Desimoni, and N. E. Christensen, Phys. B. **354**, 341 (2004).

[7] C.-M. Deng, C.-F. Huo, L.-L. Bao, X.-R. Shi, Y.-W. Li, J. Wang, and H. Jiao, Chem. Phys. Lett. **448**, 83 (2007).

[8] C.-F. Huo, Y.-W. Li, J. Wang, and H. Jiao, J. Am. Chem. Soc. **131**, 14713 (2009).

[9] S. Zhao, X.-W. Liu, C.-F. Huo, Y.-W. Li, J. Wang, and H. Jiao, Catalysis, Structure and Reactivity **1**, 45 (2015).

[10] F. Grandjean and A. Gérard, J. Phys. F **6**, 451 (1976).

[11] R. Fruchart, R. Madar, M. Barberon, E. Fruchart, and M. G. Lorthioir, J. Phys. Colloq. C1 **32**, C1-982 (1971).

[12] D. Fruchart and E. F. Bertaut, J. Phys. Soc. Jpn. **44**, 781 (1978).

[13] W. Wang, X. Kan, X. Liu, S. Feng, C. Liu, K. M. Ur Rehman, M. Shezad, Q. Wu, and Y. Wang, J. Mater. Sci.: Mater. Electron. **30**, 10383 (2019).

[14] A. Houben, J. Burghaus, and R. Dronskowski, Chem. Mater. **21**, 4332 (2009).

[15] B. S. Wang, P. Tong, Y. P. Sun, X. B. Zhu, Z. R. Yang, W. H. Song, and J. M. Dai, Appl. Phys. Lett. **97**, 042508 (2010).

[16] A. V. Gil Rebaza, J. Desimoni, S. Kurian, S. Bhattacharyya, N. S. Gajbhiye, and E. L. Peltzer y Blancá, J. Phys. Chem. C **115**, 23081 (2011).

[17] B. Qu, H. He, and B. Pan, AIP Adv. **6**, 075122 (2016).

[18] T. He, Q. Huang, A. P. Ramirez, Y. Wang, K. A. Regan, N. Rogado, M. A. Hayward, M. K. Haas, J. S. Slusky, K. Inumara, H. W. Zandbergen, N. P. Ong, and R. J. Cava, Nature **411**, 54 (2001).

[19] P. Tong, Y. P. Sun, X. B. Zhu, and W. H. Song, Phys. Rev. B **73**, 245106 (2006).

[20] M. Uehara, T. Yamazaki, T. Kori, T. Kashida, Y. Kimishima, and I. Hase, J. Phys. Soc. Jpn. **76**, 034714 (2007).

[21] V. K. Portnoi, A. V. Leonov, and S. A. Fedotov, Phys. Met. Metallogr. **107**, 276 (2009).

[22] B. He, C. Dong, L. Yang, X. Chen, L. Ge, L. Mu, and Y. Shi, Supercond. Sci. Technol. **26**, 125015 (2013).

[23] P. Tong and Y. P. Sun, Adv. Cond. Matter. Phys. 2012 Article ID 903239.

[24] D. F. Shao, W. J. Lu, S. Lin, P. Tong, H. B. Jian, X. Y. Pan, and Y. P. Sun, AIP Adv. **2**, 042167 (2012).

[25] H. M. Tütüncü and G. P. Srivastava, Philos. Mag. **93**, 4469 (2013).

[26] C. M. I. Okoye, Physica B **405**, 1562 (2010).

[27] R. Szczesniak, A. P. Durajski, K. M. Skoczylas, and Ł. Herok, J. Low Temp. Phys. **183**, v387 (2016).

[28] E. T. Dias, K. R. Priolkar, A. Das, G. Aquilanti, Ö. Çakır, M. Acet, and A. K. Nigam, J. Phys. D: Appl. Phys. **48**, 295001 (2015).

[29] E. T. Dias, A. Das, A. Hoser, S. Emura, A. K. Nigam, and K. R. Priolkar, J. Appl. Phys. **124**, 153902 (2018).

[30] Ö. Çakır, F. Cugini, M. Solzi, K. Priolkar, M. Acet, and M. Farle, Phys. Rev. B **96**, 014436 (2017).

[31] T. Tohei, H. Wada, and T. Kanomata, J. Appl. Phys. **94**, 1800 (2003).

[32] Ö. Çakır and M. Acet, Appl. Phys. Lett. **100**, 202404 (2012).

[33] Ö. Çakır and M. Acet, J. Magn. Magn. Mater. **344**, 207 (2013).

[34] Ö. Çakır, M. Acet, M. Farle, and A. Wildes, J. Phys.: Condens. Matter **28**, 13LT02 (2016).

[35] T. Harada, K. Nishimura, T. Kanomata, and T. Kaneko, Jpn. J. Appl. Phys. **32**, 280 (1993).

[36] J. Rodriguez-Carvajal, Physica B **192**, 55 (1993).

[37] Y. Zhao, H. Su, K. Sun, J. Liu, and W. Li, Surf. Sci. **606**, 598 (2012).

[38] Y. Li, Y. Gao, B. Xiao, T. Min, Y. Yang, S. Ma, and D. Yi, J. Alloys Compd. **509**, 5242 (2011).

[39] X. Chong, Y. Jiang, R. Zhou, and J. Feng, Comput. Mater. Sci. **87**, 19 (2014).

[40] C. M. Fang, M. A. van Huis, and H. W. Zandbergen, Phys. Rev. B **80**, 224108 (2009).

[41] H. I. Faraoun, Y. D. Zhang, C. Esling, and H. Aourag, J. Appl. Phys. **99**, 093508 (2006).

[42] M. K. Chattopadhyay, S. B. Roy, and P. Chaddah, Phys. Rev. B **72**, 180401(R) (2005).

[43] Ö. Çakır, M. Acet, M. Farle, E. Dias, and K. Priolkar, J. Magn. Magn. Mater. **390**, 96 (2015).

[44] A. Tekgül, M. Acet, M. Farle, and N. Ünal, J. Alloys Compd. **695**, 418 (2017).